10

Oceanic Evaporation: Trends and Variability

Long S. Chiu[1], Si Gao[1] and Chung-Lin Shie[2]
[1]*Department of Atmospheric, Oceanic and Earth Sciences, George Mason University*
[2]*UMBC/JCET, NASA/GSFC*
USA

1. Introduction

The global water and energy cycles are strongly coupled as two essential components of earth system. They play important roles in altering the Earth's climate.

Oceanic evaporation, or sea surface latent heat flux (LHF) divided by latent heat of vaporization (L_v), is a key component of global water and energy cycle. In a bulk aerodynamic formulation, it is determined by the transfer coefficient of evaporation, C_E, and bulk parameters such as surface wind speed (U), surface saturated and near-surface air specific humidity (Q_s and Q_a),

$$LHF = \rho L_v C_E U(Q_s - Q_a) \tag{1}$$

where sea surface saturated humidity is determined by sea surface temperature (SST) and salinity, and ρ is density of moist air. The transfer coefficient is dependent on the stability of the atmosphere and the sea state (Liu et al., 1979; Zeng et al., 1988). Historically, marine surface observations have provided the basis for estimating these oceanic turbulent fluxes (e.g. Bunker, 1976; Cayan, 1992; da Silva et al., 1994; Esbensen & Kushnir, 1981; Hastenrath, 1980; Hsiung, 1985; Isemer & Hasse, 1985, 1987; Josey et al., 1998; Oberhuber, 1988; Renfrew et al., 2002; Weare et al., 1981). The advent of remote sensing techniques offers means to retrieve a number of surface bulk variables. Microwave radiation interacts directly with water molecules and hence is effective in providing water vapor information. The sea surface emissivity is affected by the sea state and foam conditions, which is related to surface wind. For instance, global microwave measurement of the Special Sensor Microwave Imager (SSM/I) on board a series of Defense Meteorological Satellite Program (DMSP) satellites has been used to retrieve near-surface air humidity and winds over the ocean.

At present there are several remote sensing products of global ocean surface latent heat flux. They include the NASA/Goddard Satellite-based Surface Turbulent Flux (GSSTF) dataset version 1 (Chou et al., 1997) and version 2 (GSSTF2, Chou et al., 2003), the Japanese Ocean Flux utilizing Remote Sensing Observations (J-OFURO) dataset (Kubota et al., 2002) and the Hamburg Ocean Atmosphere Parameters and Fluxes from Satellite (HOAPS) dataset (Grassl et al., 2000). Chiu et al. (2008) examined "trends" and variations in these global oceanic evaporation products for the period 1988–2000. They found a long-term increase in global average LHF that started around 1990 in GSSTF2. They argued that the dominant patterns may be related to an enhancement of Hadley circulation and El Niño-Southern Oscillation

(ENSO), respectively. An updated version of SSM/I version 6 (V6) data released by Remote Sensing Systems (RSS) in 2006 [as used by Wentz et al. (2007), see http://www.ssmi.com] that calibrates all SSM/I sensors is available in 2008. Shie et al. (2009) have reprocessed and forward processed GSSTF2 to version 2b (GSSTF2b, Shie et al. 2010; Shie 2010) using the SSM/I V6 data (including total precipitable water, brightness temperature, and wind speed retrieval), covering the period July 1987–December 2008. We provide an assessment of these data products and examine their "trends" and variability.

The data and methodology are described in Section 2. Section 3 presents the trends of these products, compares GSSTF2 and GSSTF2b for the pre 2000 periods, assesses the post 2000 performance, and examines the GSSTF2b Set1 and Set2 differences. Summary and discussion are presented in Section 4.

2. Data and methodology

Earlier version of these flux products have been described elsewhere (Chiu et al., 2008). The product versions described here represent the most updated versions as of the writing of this report.

2.1 HOAPS

Detail descriptions of the latest version of HOAPS, (version 3, or HOAPS-3) are given in Andersson et al. (2010). Bulk variables are derived from SSM/I data except for the SST which is derived from the Advanced Very High Resolution Radiometer (AVHRR) Oceans Pathfinder SST product. A neural network algorithm is used to derive U. The Q_a is obtained using the linear relationship of Bentamy et al. (2003). The Q_s is computed from the AVHRR SST using the Magnus formula (Murray, 1967) with a constant salinity correction factor of 0.98. The near-surface air temperature (T_a) is estimated from the SST using the assumptions of 80% constant relative humidity and a constant surface-air temperature difference of 1 K. Latent and sensible heat fluxes are calculated using the Coupled Ocean–Atmosphere Response Experiment (COARE) 2.6a bulk algorithm (Fairall et al., 1996, 2003).

The HOAPS-3 data sets cover the time period from July 1987 to December 2005. HOAPS-G pentad and monthly data sets with 0.5-degree resolution and HOAPS-C twice daily data set with 1-degree resolution are available at the website (http://www.hoaps.zmaw.de).

2.2 J-OFURO

The updated version of J-OFURO, (version 2, J-OFURO2) is described in Tomita et al. (2010). Bulk variables U, Q_a and SST (Q_s) are determined by multi-satellite and multiple satellite sensors. U is obtained from a combination of microwave radiometers (SSM/I, AMSR-E and TMI) and scatterometers (ERS-1, ERS-2 and QuikSCAT). Q_a is derived from SSM/I measurements. SST is taken from the Merged satellite and in-situ data Global Daily SST (MGDSST, Sakurai et al. 2005) analysis provided by Japanese Meteorological Agency (JMA). T_a is obtained from NCEP/DOE reanalysis. COARE 3.0 bulk algorithm (Fairall et al., 2003) is used to estimate LHF and SHF. The J-OFURO2 covers the time period from January 1988 to December 2006. Daily and monthly means with 1-degree resolution are available at the website (http://dtsv.scc.u-tokai.ac.jp/j-ofuro).

2.3 GSSTF

The GSSTF2 product has daily and monthly fields with a 1°x1° resolution for July 1987–December 2000 (Chou et al., 2001), based on the method of Chou et al. (1997) with some improvements (Chou et al., 2003). The temporal and spatial resolutions of GSSTF2b are the same as those of GSSTF2, except that GSSTF2b product covers a longer period (July 1987–December 2008).

GSSTF2b dataset is processed using improved input datasets, namely the recently released NCEP SST analysis, and a uniform (across satellites) surface wind and microwave brightness temperature (TB) V6 dataset from the SSM/I produced by RSS. Table 1 summarizes characteristics of input data and parameters for HOAPS3, J-OFURO2, GSSTF2 and GSSTF2b, in that order. As we focus on LHF, only detailed descriptions and discussions on input parameters of LHF are presented.

A major improvement in the input parameters of GSSTF2b is the use of the newly released SSM/I V6 product (see discussions in http://www.ssmi.com). The SSM/I V6 product removes the spurious wind speed trends found in the Wentz/RSS SSM/I V4 wind speed retrievals. To be consistent, the SSM/I V4 total precipitable water (*W*) and bottom-layer precipitable water (*WB*) used in GSSTF2 are replaced by the corresponding SSM/I V6 products in the production of GSSTF2b. Moreover, the weekly 1° spatial resolution Optimum Interpolation (OI) SST version 1 (V1) dataset (Reynolds & Smith, 1994) used in GSSTF2 is replaced by the improved OI SST version 2 (V2) dataset. The OI SST V2 has a lower satellite bias, a new sea ice algorithm, and an improved OI analysis (Reynolds et al., 2002) resulting in a modest reduction of the satellite bias and global residual biases of roughly −0.03°C. The major improvement in the V2 analysis shows up at high latitudes where local differences between the old and new analysis can exceed 1 °C due to the application of a new sea ice algorithm. There are two GSSTF2b sets, Set1 and Set2 (Shie et al., 2010; Shie 2010). Set1 is developed using all available DMSP SSM/I sensor data. In a preliminary analysis, it was noted that there are large trends associated with LHF which are mostly attributed to the DMSP F13 and F15 satellites. Set2 was produced by excluding satellite retrievals that are judged to caused relatively large artificial trends in LHF (mostly post 2000) from Set1. Consequently Set2 is identical to Set1 before 1997 and shows a smaller trend than Set1 for the whole period, while Set1 has better spatial coverage (less missing data). Hilburn & Shie (2011) further found a drift in the Earth incidence angle (EIA) associated with the SSM/I sensors on the DMSP satellites that introduces artificial trends in the SSM/I TB data. These artificial trends introduce large changes in the boundary water (*WB*), which affects the Q_a, and thus the LHF retrievals. An improved version, GSSTF2c, incorporating the corrected SSM/I brightness temperature, has been produced as of this writing (Shie et al., 2011). The retrieved *WB*, Q_a and LHF have genuinely improved, particularly in the trends post 2000 (Shie & Hilburn, 2011). An extensive study involving the GSSTF2c will be presented in a separate paper.

In this chapter, "trend" is used to indicate results from linear regression analysis and/or Empirical Mode Decomposition (EMD) for the period of study. Linear regression of the time series with time is used to detect linear trends and the significance can be estimated from the slope of the regression. EMD is based on local characteristic time scales of the data and is therefore applicable for analyzing nonlinear and non-stationary processes (Huang et al., 1998). It decomposes the time series into a finite and often small number of intrinsic mode

Datasets	HOAPS3	J-OFURO2	GSSTF2	GSSTF2b
C_E (transfer coefficient)	Fairall et al. (1996, 2003)	Fairall et al. (2003)	Chou (1993)	Chou (1993)
U (speed)	SSM/I V6 TB and neural network algorithm	SSM/I, AMSR-E, TMI, ERS-1, ERS-2 and QuikSCAT	Wentz V4 (1997)	Wentz V6 (2007)
U (vector)	N/A	N/A	Atlas et al. (1996)	CCMP Level-2.5 (SSM/I, TMI, and AMSR-E)
W/*WB*	N/A	N/A	Wentz V4 (1997)	Wentz V6 (2007)
SST	AVHRR	MGDSST Sakurai et al. (2005)	NCEP/NCAR Reanalysis (V1) Reynolds & Smith (1994)	NCEP/DOE Reanalysis (V2) Reynolds et al. (2002)
Q_a	Bentamy et al. (2003)	Schlussel et al. (1995)	Chou et al. (1995, 1997)	Chou et al. (1995, 1997)
T_a	Estimated from SST with assumptions of 80% humidity and 1 K surface-air temperature difference	NCEP/DOE Reanalysis (V2)	NCEP/NCAR Reanalysis (V1)	NCEP/DOE Reanalysis (V2)
Spatial resolution	1°x1°, 0.5°x0.5°	1°x1°	1°x1°	1°x1°
Spatial coverage	Global Oceans	Global Oceans	Global Oceans	Global Oceans
Temporal resolution	Twice daily, pentad and monthly	Daily and monthly	Daily and monthly	Daily and monthly
Temporal coverage	Jul. 1987 – Dec. 2005	Jan. 1988 – Dec. 2006	Jul. 1987 – Dec. 2000	Jul. 1987 – Dec. 2008

Table 1. Characteristics of input data and parameters for HOAPS3, J-OFURO2, GSSTF2 and GSSTF2b.

functions (IMFs) of increasing time scales. The existence of a trend is dependent on the length of the dataset. If the last IMF (one with longest time scale) is monotonically increasing or decreasing, a trend is indicated. The EMD is a more stringent test for significance of "trends."

Non-seasonal variability is examined using Empirical Orthogonal Function (EOF) analysis. Non-seasonal data are obtained by subtracting the monthly climatology of the study period from the monthly data. EOF analysis decomposes a spatio-temporal dataset into a series of orthogonal spatial EOF patterns and the associated time series (also called principal components). The test proposed by North et al. (1982) is used to judge the EOFs to see if they are significant and distinct. To examine the significance of each EOF, the logarithm of

the variance explained by the EOF is plotted against its EOF number. The variance explained by the nth EOF is given by $\lambda_n / \sum_{i=1}^{N} \lambda_i$ where λ_n is the nth eigenvalue and N is the number of time samples. Linear regression between the logarithms of λ_n vs n is computed. EOFs above the regression line are judged to be significant.

3. Results

3.1 Global and zonal average

Figure 1 shows the area weighted global (60°N–60°S) average LHF of HOAPS3, J-OFURO2, GSSTF2, and Set1 and Set2 of GSSTF2b. The merged OAFLUX product is included for comparison. Visual inspection of the data products does not show large missing gaps in the spatial distribution of the products. All satellite products-HOAPS3, J-OFURO2 and all GSSTF datasets show increases while there is no obvious trend in OAFLUX. All products have similar global means in the early period 1988–1991. The means of GSSTF2b (both Set1 and Set2) are generally lower than that of GSSTF2 which is the highest among all products. All products show a dip in 1991 and an increase afterwards. The dip is clearly evident in HOAPS3. GSSTF2b Set1 and Set2 are identical up to 1998 after which they diverge, but tend to come close again after 2006.

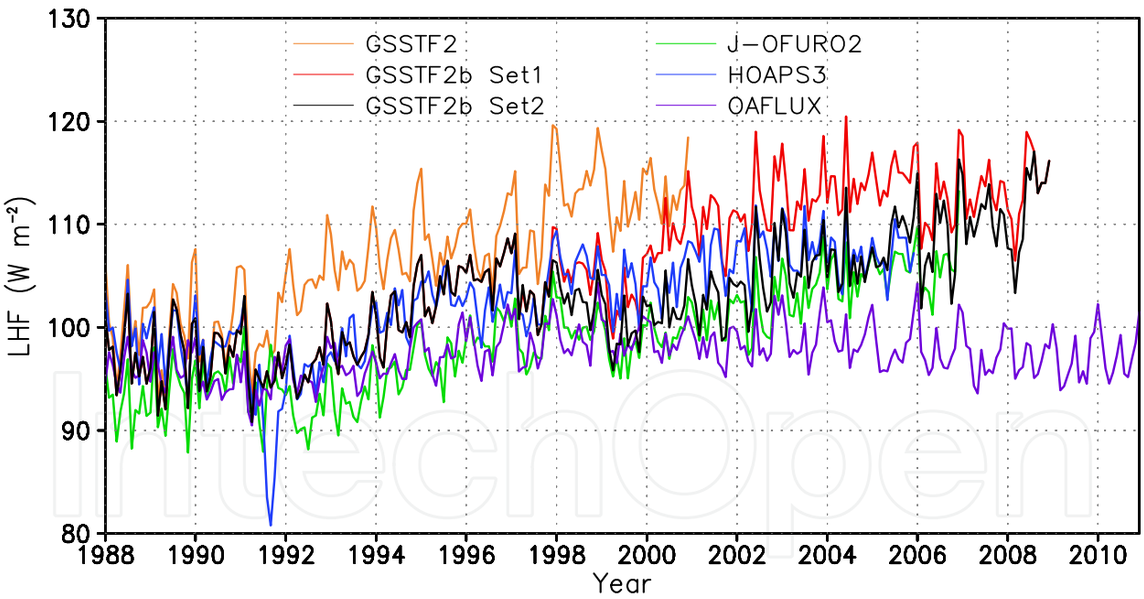

Fig. 1. Time series of global (60°N–60°S) oceanic average latent heat flux derived from HOAPS3, J-OFURO2, GSSTF2, GSSTF2b Set1 and Set2 and OAFLUX.

The zonal annual averages of LHF are depicted in Figure 2. The general features of the zonal means are quite similar among these products: they showed maxima in the subtropics, minima at the poles and relative minima at the equator. The subtropical maxima in the southern hemisphere are slighter higher than those in the northern hemisphere for the same product. While GSSTF2 is the highest among these estimates, the

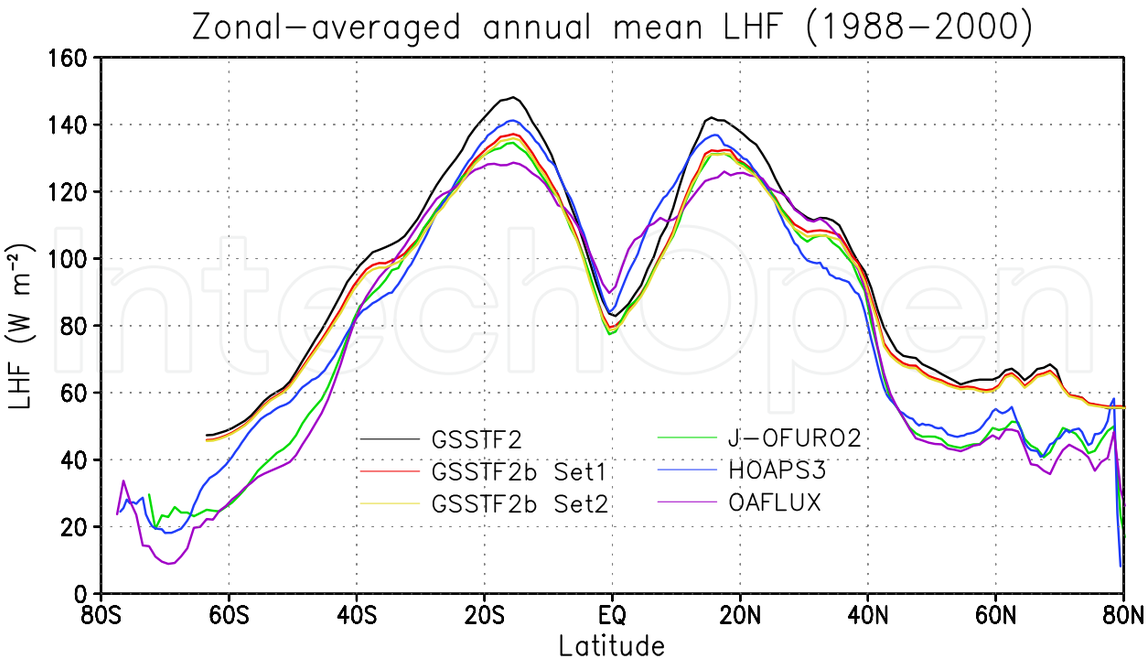

Fig. 2. Zonal annual mean of LHF for oceanic evaporation computed from HOAPS3, J-OFURO2, GSSTF2, GSSTF2b Set1 and Set2 and OAFLUX.

GSSTF2b Set2 is slightly lower than HOAPS3 but higher than J-OFURO2 and OAFLUX at their maxima. Poleward of 30°, the GSSTF zonal means are generally higher than the other products.

3.2 Trend analysis

Linear regression analyses of the time series with time were performed on the global mean time series. The significance of the slopes of the regression (trend) is tested using a t-test. The degree of freedom for the significance test takes into account the serial correlation of the time series (Angell, 1981; Chiu & Newell, 1983). GSSTF2 shows the largest trend. It is followed by GSSTF2b Set1 while the GSSTF2b Set2 trend is comparable to HOAPS3 and J-OFURO2 for the period of overlap (1988–2005). OAFLUX exhibits the smallest trend. Table 2 summarizes our results.

To map out the geographic differences, Figure 3 compares the spatial distribution of linear trends of GSSTF2b Set1 and Set2, HOAPS3, J-OFURO2 and OAFLUX. The linear trends are calculated for the common time period 1988–2005. While the magnitudes of the trends are different, the locations of maximum change are similar among HOAPS3, J-OFURO2 and GSSTF2b Set1 and Set2 - all show increasing trends in the storm tracks in the north Atlantic and north Pacific, the oceanic dry zones off the Inter-tropical Convergence Zone (ITCZ) in the western south Pacific and in latitude bands between 30−40°S off the coast of Australia and in the Indian Ocean. OAFLUX shows increasing trends in the storm tracks in both the North Atlantic and North Pacific, and in the eastern coastal regions off South America and Australia. There are large areas showing a decrease, notably in the south Indian Ocean, tropical eastern North Pacific and in North Atlantic.

Period	GSSTF2	GSSTF2b Set1	GSSTF2b Set2	HOAPS3	J-OFURO2	OAFLUX
1988–2000	10.44	9.88	5.98	7.75	6.51	3.71
1988–2005	N/A	11.69	6.34	7.35	7.62	2.41
1988–2008	N/A	10.45	7.08	N/A	N/A	1.50

Table 2. Linear trends of LHF products (in W m^{-2} decade^{-1}) for the different periods. All values are significant at 99% level.

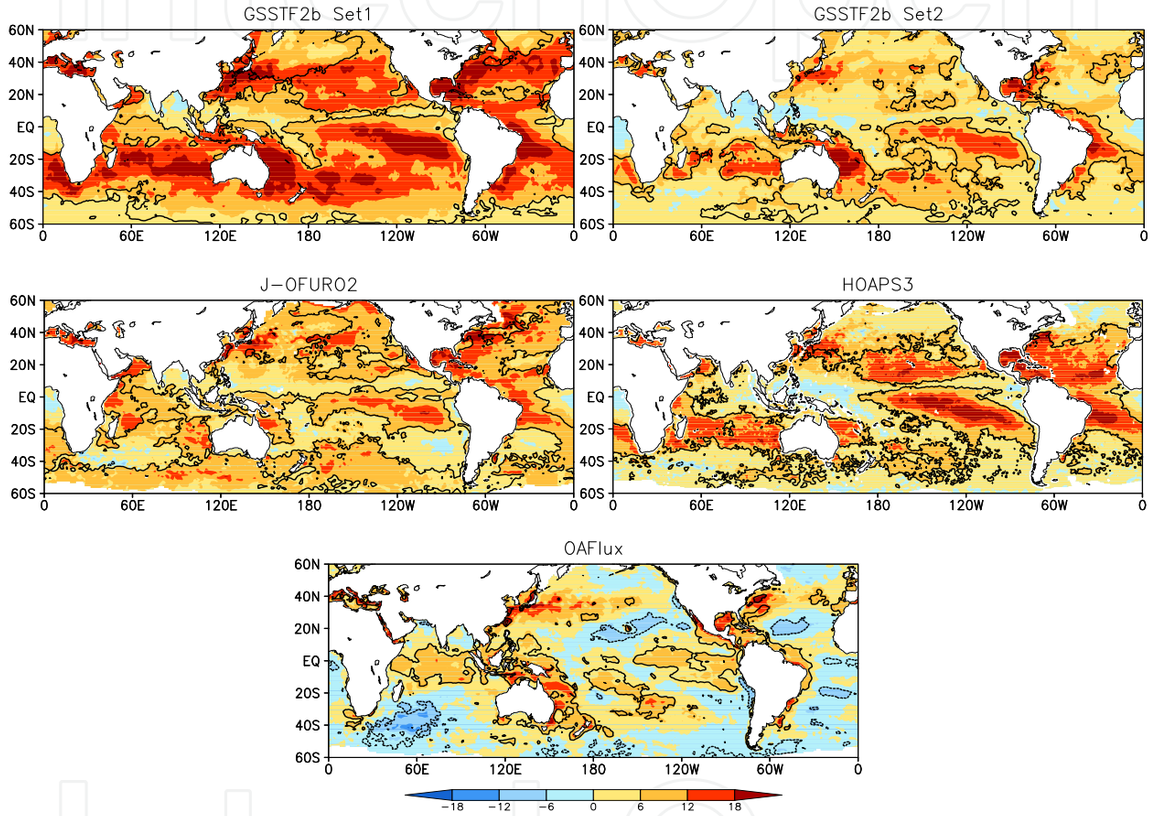

Fig. 3. Linear trends of LHF (W m^{-2} decade^{-1}) over the period 1988–2005. Contours give the trends above 95% confidence level.

3.3 EMD analysis of global average LHF

We performed EMD analyses for both GSSTF2 and GSSTF2b for the periods 1988–2000 and 1988–2008, respectively. Figure 4 shows the last IMFs from EMD analysis of GSSTF2b global average (60°N–60°S) LHF for the period 1988–2008, along with those of HOAPS3, J-OFURO2 and OAFLUX. EMD analysis of GSSTF2 global average LHF for the period 1988–2000 (Chiu et al., 2008; Xing, 2006) showed an increase starting around 1990 before the Mt Pinatubo eruption event in 1991. The last IMF of GSSTF2b Set2 and HOAPS3 show a dip around 1990 while J-OFURO2 and GSSTF2b Set1 show monotonic increases. From EMD analysis, a "trend" cannot be ascertained for the whole period for GSSTF2b Set2 and HOAPS3.

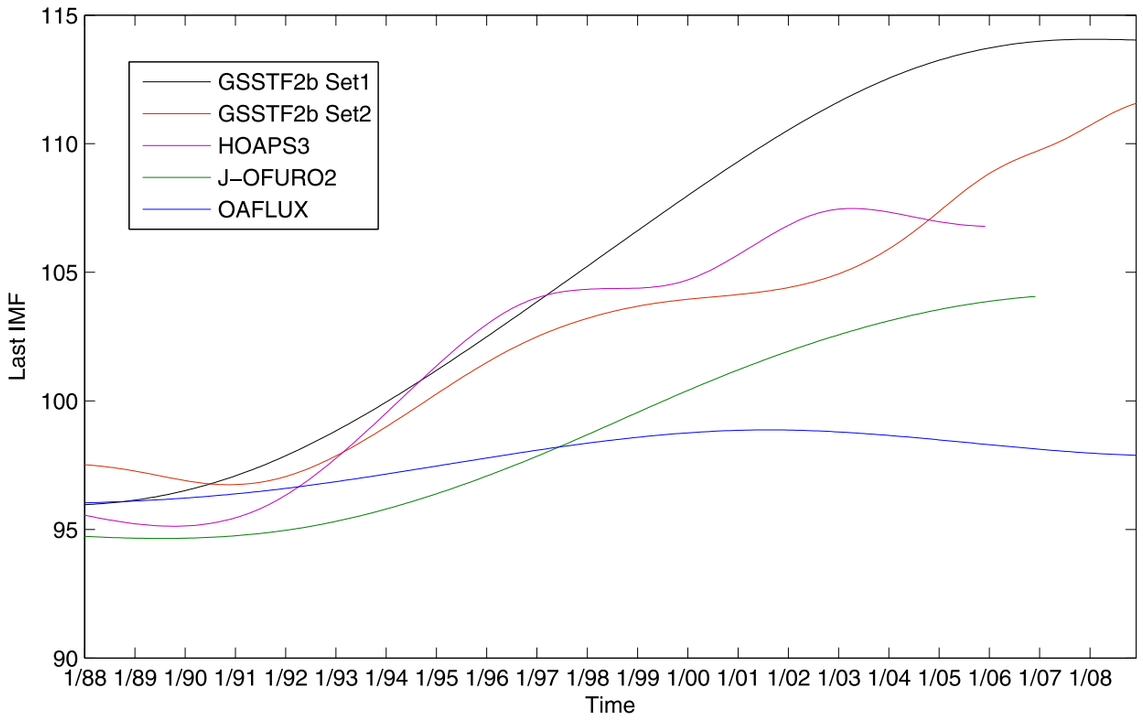

Fig. 4. The last IMFs (W m^{-2}) from EMD analysis of global (60°N–60°S) average LHF for GSSTF2b Set1 (black), GSSTF2b Set2 (red), and OAFLUX (blue) for the period 1988–2008, HOAPS3 (purple)for the period 1988–2005 and J-OFURO2 (green) for the period 1988–2006.

3.4 GSSTF2b Set1 and Set2

In this subsection, we analyze the difference between GSSTF2b Set1 and Set2. The linear trends of GSSTF2b LHF for the entire period 1988–2008 are depicted in Figure 5. The magnitudes of the trends are reduced when compared to GSSTF2 (see Chiu et al., 2008) and Set1 shows larger trends than Set2, as anticipated.

Trends of the zonal averages are shown in Figure 6. Both Set1 and Set2 show similar trend patterns while the magnitude in Set2 is much reduced. Maximum increasing trends are located in the subtropics, with maxima at 30°S and 35°N, poleward of the latitude of maximum zonal evaporation, while the trend at the thermal equator (~5°N) shows a minimum.

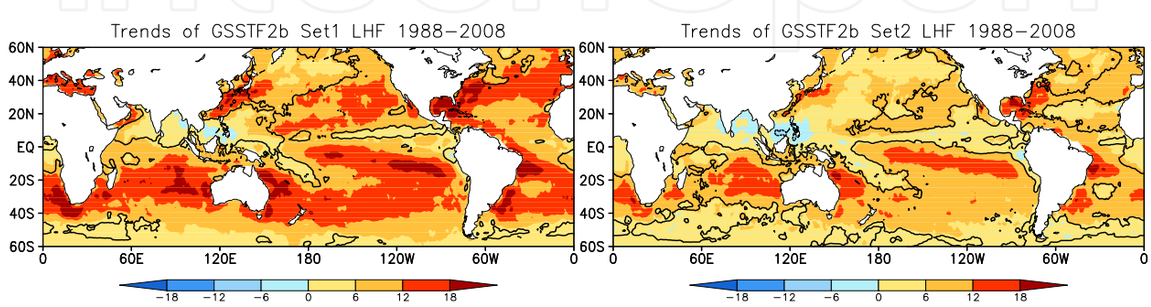

Fig. 5. Linear trends of GSSTF2b Set1 and Set2 LHF (1988–2008). Unit in W m^{-2} decade^{-1}. Contours give the trends above 95% confidence level.

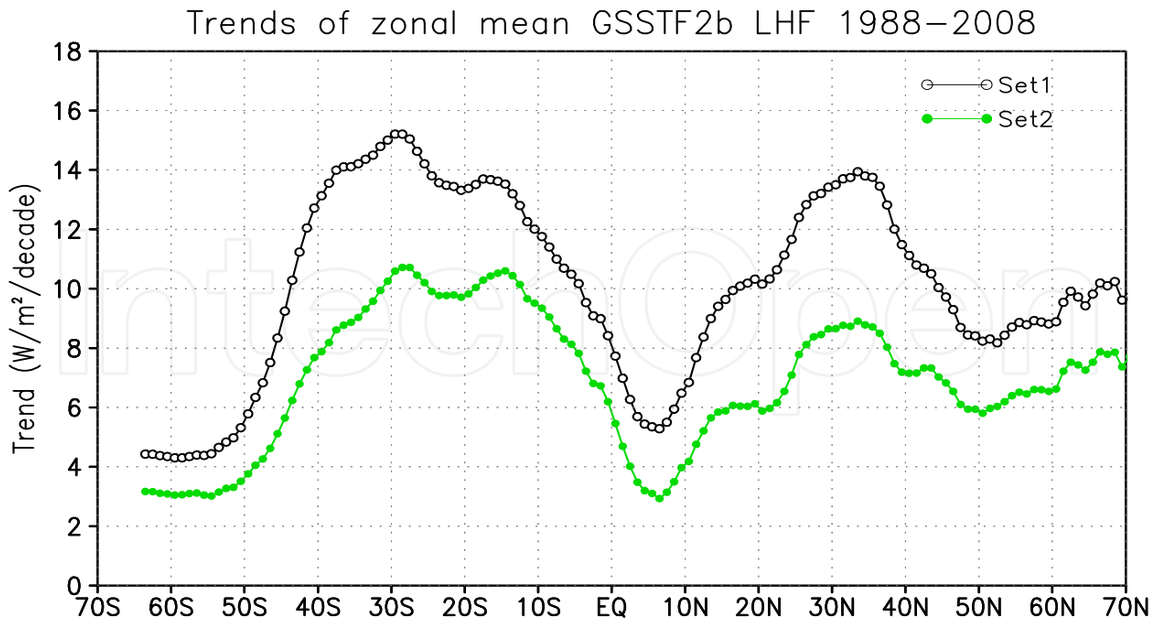

Fig. 6. Linear trends of zonal mean GSSTF2b Set1 and Set2 LHF.

Figure 7 shows the spatial distribution of trends in U, DQ and Q_a in Set 1 and Set2. It can be seen that the trend pattern in U is almost identical in both Set1 and Set2. Major difference is found in the DQ field, the magnitudes of the trends in Set1 are larger than that in Set2. In the equatorial eastern Pacific, in portion of the South China Sea, and the Bay of Bengal, Set2 actually shows a decreasing but non-significant trend. For the Q_a trend, Set1 shows large areas of decreases. While the patterns are similar for Set2, the magnitudes are much reduced, and in some areas, such as the eastern North Pacific and the bulk of the North Atlantic, the decreasing trends actually reverse to increasing trends.

LHF is a product of the surface wind (U) and the humidity difference (DQ=Q_s–Q_a) if we assume the variation in C_E is small (Equation 1). Judging from the change pattern of U and DQ they are essentially decoupled. Equation (1) can be integrated globally to get

$$\frac{\delta\overline{LHF}}{\overline{LHF}} \approx \frac{\delta\overline{U}}{\overline{U}} + \frac{\delta\overline{DQ}}{\overline{DQ}} \tag{2}$$

$$\delta\overline{DQ} = \delta\overline{Q_s} - \delta\overline{Q_a} \tag{3}$$

where δx represent the change in the quantity x, $\delta x/x$ represent fractional changes in x, and the over-bar $\overline{x}$ represents global average of x. For GSSTF2 (1988–2000), the terms in equation (2) is approximately 17%, 6%, and 11%, in that order (Xing, 2006). Most of the increase in $\overline{DQ}$ was attributed to increase in $\overline{Q_s}$ and decrease in $\overline{Q_a}$.

Figure 8 shows the time series of global average U, DQ and Q_a for GSSTF2b Set1 and Set2, respectively. It clearly indicates the divergence of Set1 and Set2 in late 1997. The large difference in LHF between Set1 and Set2 is mostly attributed to DQ, which is due to the higher Q_a in Set2. The difference in U between the datasets is small. There is a large decrease in Q_a at the end of 2008.

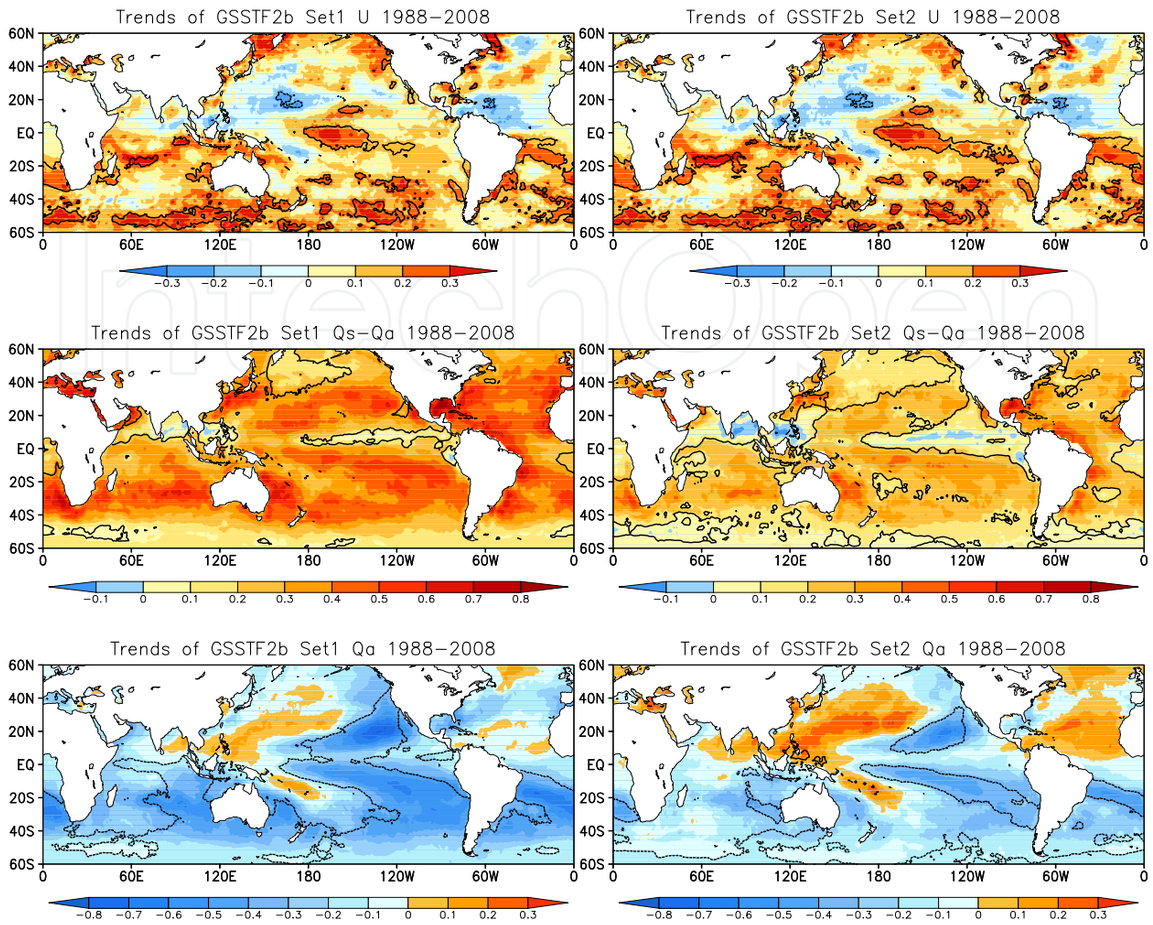

Fig. 7. Linear trends of surface wind speed (U, upper panel), surface humidity difference (DQ=Q_s–Q_a, middle panel), and surface air humidity (Q_a, lower panel) for GSSTF2b Set1 (left column) and Set2 (right column). Units are in m s^{-1} decade^{-1} for U and in g kg^{-1} decade^{-1} for DQ and Q_a. Contours give the trends above 95% confidence level.

Table 3 shows the changes in LHF in Set1 and Set2 of GSSTF2b (1988–2008) and the associated changes in U, DQ and the changes in Q_s and Q_a. The change in DQ contribute most to the change in LHF for both Set1 and Set2, while the changes in DQ is due both to an increase in Q_s and decrease in Q_a. The difference in the change of LHF between Set1 (23.1%) and Set2 (15.5%) is mostly attributed to DQ (20.0% vs. 12.3%) and changes in Q_a (–0.51 g kg^{-1} vs. –0.24 g kg^{-1}). It is clear that the impact of DMSP F13 is the introduction of a much lower Q_a, thus affecting DQ and ultimately LHF.

	$\frac{\delta\overline{LHF}}{\overline{LHF}} \approx \frac{\delta\overline{U}}{\overline{U}} + \frac{\delta\overline{DQ}}{\overline{DQ}}$	$\frac{\delta\overline{U}}{\overline{U}}$	$\frac{\delta\overline{DQ}}{\overline{DQ}}$	$\delta\overline{DQ}$ (g kg^{-1})	$\delta\overline{Qs}$ (g kg^{-1})	$\delta\overline{Qa}$ (g kg^{-1})
Set1	23.1%	3.1%	20.0%	0.73	0.22	–0.51
Set2	15.5%	3.1%	12.3%	0.46	0.22	–0.24

Table 3. Summary of changes in LHF, U and DQ and Q_s and Q_a for GSSTF2b Set1 and Set2.

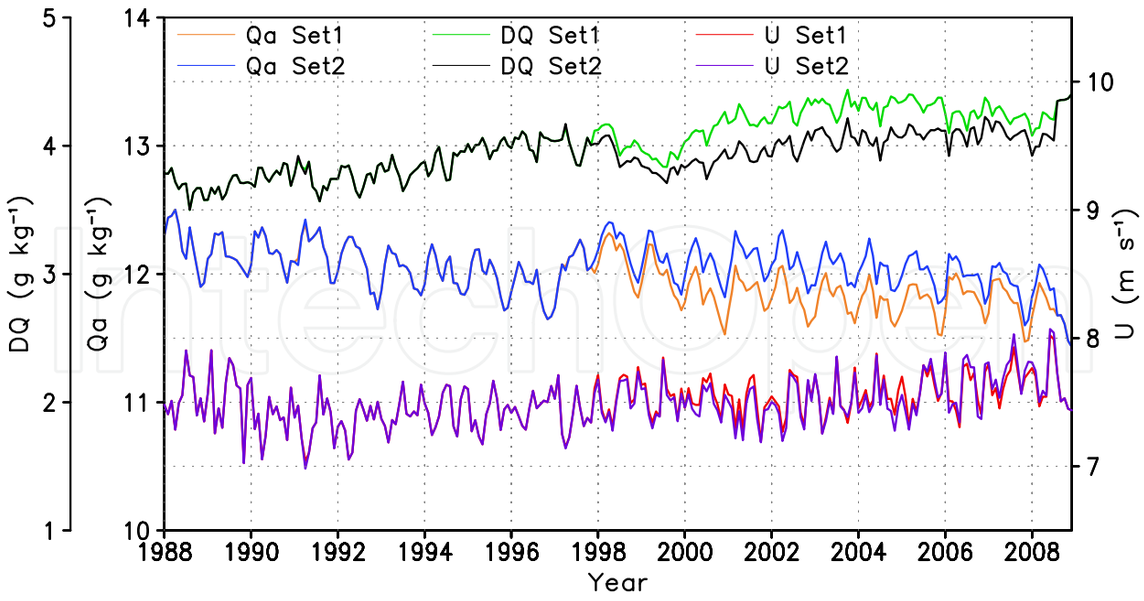

Fig. 8. Time series of global average surface humidity difference (DQ), surface air humidity (Q_a) and wind speed (U) for GSSTF2b Set1 and Set2.

3.5 EOF analyses and teleconnections

Empirical Orthogonal Function (EOF) analyses are performed on LHF of both GSSTF2b Set1 and Set2 for the period 1988–2008. Monthly means for the entire period are first removed from the data to form the non-seasonal dataset. The first, second and third EOF of Set1

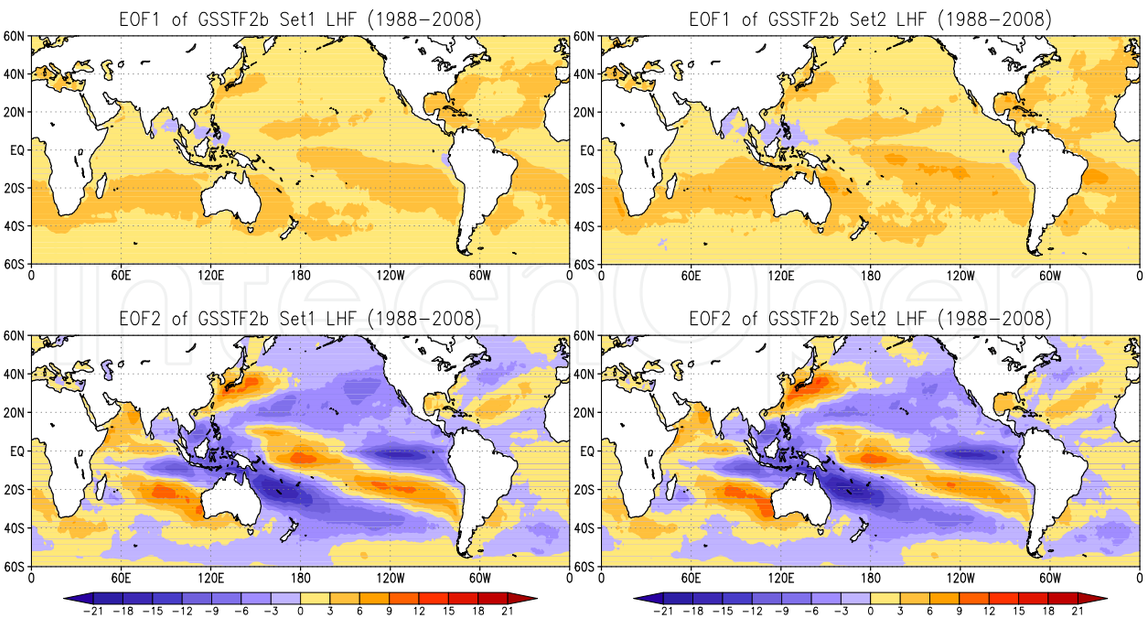

Fig. 9. Spatial patterns of the first (top) and second (bottom) EOF of GSSTF2b LHF for the period 1988–2008. The variances explained are 8.6% (11.5%) and 4.3% (4.3%) for EOF1 and EOF2 for Set2 (Set1), respectively.

explains 11.5%, 4.3%, and 3.4% of the total variance, and the corresponding variance explained for Set2 are 8.6%, 4.3% and 3.4%. Figure 9 shows the spatial patterns of the first (EOF1) and second (EOF2) EOF for Set1 and Set2, respectively. Their associated time series, accompanied by a rescaled Southern Oscillation Index (SOI), are presented in Figure 10. The general patterns of EOF1 of Set1 and Set2 are very similar, with large weights in subtropical Indian Ocean, the dry zone in the eastern tropical South Pacific and South Atlantic. They also bear striking resemblance to the first EOF pattern computed from GSSTF2 which shows

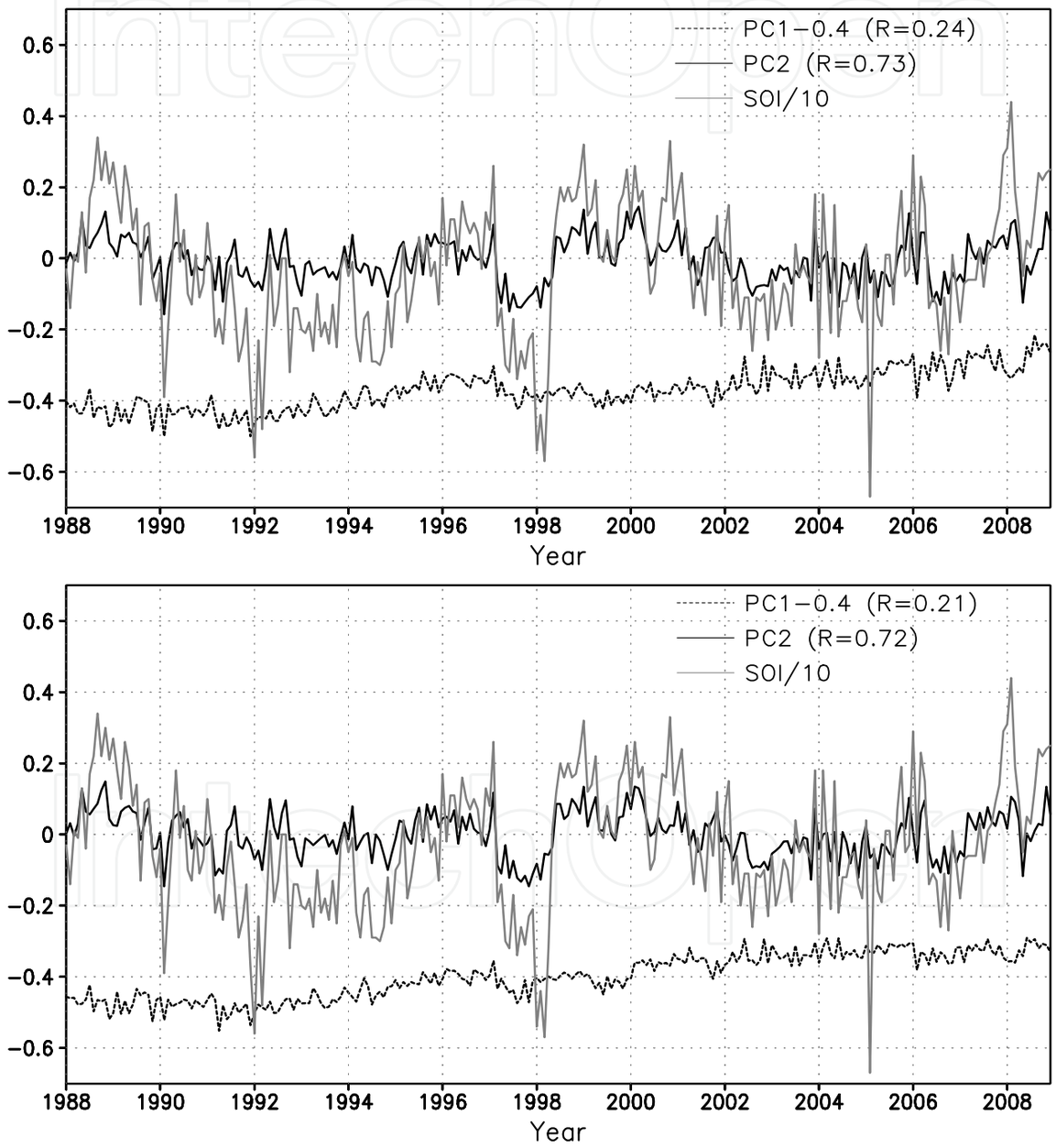

Fig. 10. Time series associated with EOF of non-seasonal GSSTF2b Set2 LHF for the period 1988–2008 and the SOI for the same period. The SOI is divided by 10 and the time series of the first EOF is shifted by –0.4 units for clarity. The lower panel shows the same for Set1.

weights of the same sign everywhere (Chiu et al., 2008). However, in GSSTF2b, there are regions of opposite sign in the South China Sea area in both Set1 and Set2, with higher weights in Set2 in the centers of highs. The EOF2 patterns for Set1 and Set2 are almost identical. Similarity is also noted for the EOF2 pattern derived from GSSTF2 (Chiu et al., 2008).

The time series of EOF1 also show a slight increasing trend, suggesting an increase of LHF over most of the global ocean. The associated time series of EOF2 have a significant correlation of 0.73 (0.72 for Set1) with SOI, reaffirming that EOF2 - ENSO events association.

The third EOF pattern (not shown) is characterized by a negative - positive - negative (– + –) zonal changes centering around 10−20°N, 20−30°N and north of 40°N in the north Pacific and a (+ – +) centering at 20°N, 30°N and 50°N in the North Atlantic. The pattern correlations for EOF1, EOF2 and EOF3 between Set1 and Set2 are 0.08, 0.49, and 0.39, and the corresponding temporal correlation for the associated time series are 0.92, 0.97, and 0.83, in that order.

EOF3 is reminiscent of the North Atlantic Oscillation (NAO) and the North Pacific Oscillation (NPO) patterns (Walker & Bliss, 1932; Wallace & Gultzer, 1981, Hurrell et al., 2003). These teleconnection patterns are further discussed in terms of an atmospheric annular mode, or Arctic Oscillation (AO), showing the opposition between subtropical highs and the polar lows (Wallace, 2000; Deser, 2000; Aubaum et al., 2001). We compute the correlations between an AO index with the time series of EOF3 and found no significant correlation with Set2, however a correlation of 0.32 is found for EOF3 Set1, significant at 95% level.

4. Summary and discussion

Four satellite based sea surface latent heat flux (LHF) products, HOSAPS3, J-OFURO2, GSSTF2, and GSSTF2b (Set1 and Set2) and a merged analysis OAFLUX are compared. Linear trend analysis of all satellite based products show large increasing trend, with GSSTF2 the largest, followed by GSSTF2b Set1, J-OFURO2, HOAPS3, and GSSTF2b Set2. OAFLUX exhibits the lowest linear increasing trend. Most of the satellite products used SSM/I as input. Small drifts in the SSM/I brightness temperature (TB) associated with changes in Earth incidence angle (EIA) was noted in most of the SSM/I data (Hilburn & Shie, 2011; Shie & Hilburn, 2011). Because of the sensitivity of the boundary layer water (*WB*) to the TB, these small drifts can introduce artificial trends in bulk quantities such as Q_a. A second data set, GSSTF2b Set2, which excludes satellite retrievals that were judged to introduce these biases, was introduced. The most-excluded satellite data are SSM/I onboard the DMSP F13 and F15 satellites. The new set, GSSTF2b Set2, was found to have a much reduced increasing trend, the magnitude of which is comparable to HOAPS3 and J-OFURO2 for the period of overlap. To account for the drift in the EIA, a new version of GSSTF, GSSTF2c, that takes account of the correction in EIA, has been completed as of this writing, and will be officially released to the public via NASA/GES DISC by the end of October 2011 (Shie et al., 2011). These trend issues will be revisited after its release.

Empirical Mode Decomposition (EMD) analyses, which are designed for examining non-stationary non-homogeneous time series, are performed on the global LHF. The last IMF of GSSTF2b Set1 shows a monotonic increase indicating the existence of a trend in this period.

The corresponding IMF of the other data products do not show monotonic increases, hence trends cannot be ascertained.

To examine the attribution of the increase in GSSTF2b Set1 and Set2, the linear trends in both the surface wind (U) and surface humidity difference (DQ) are computed. There is no significant difference between the trend patterns in the wind field. However, large difference in the DQ trend is noted. The DQ trend difference is attributed to a reduction in the negative trend in surface air humidity (Q_a) in Set2.

A major difference between GSSTF2 and GSSTF2b is the use of RSS SSM/I V4 for GSSTF2 and RSS SSM/I V6 for GSSTF2b. The changes in LHF, U, and DQ are 16%, 6%, and 11% for GSSTF2 (Xing, 2006). The corresponding changes are 23%, 3%, and 20% for GSSTF2b Set1 and 16%, 3%, and 12% for Set2 (Table 3). The use of RSS SSM/I V6 products reduces the wind trend from 6% to 3% but increases the DQ trend from 11% to 20% for Set1. The exclusion of F13 and F15 data reduces the LHF trend to 16%, mostly due to a reduction in the DQ trend to 12% (from 20%) with U changes remain at 3%.

Interannual variability is examined using EOF analyses. The first three significant non-seasonal EOF patterns are similar, and they explaining 10.5%, 4.3% and 3.4% for Set1 and 8.6%, 4.3% and 3.4% for Set2, respectively. The first EOF pattern of GSSTF2 for 1998–2000, with opposite changes between the equatorial eastern Pacific and the subtropics in the Pacific and Indian ocean, may be indicative of an enhance Hadley circulation (Chiu & Xing, 2004; Chiu et al., 2008). Observations also indicate large decadal variability in the Hadley Circulation (Wielicki et al., 2002; Cess & Udelhofen, 2003; Chen et al., 2002; Mitas and Clements, 2005).

This seesaw pattern is much reduced in the EOF1 pattern in both GSSTF2b Set1 and Set2 of 1998–2008, which may indicate a reduction, change of phase, or mixing of the signal with the trend in GSSTF2b. The contribution to the total variance is smaller for Set2, which excluded DMSP datasets that contains large long-term trends introduced by drifts in the Earth incidence angle in the SSM/I sensors. The difference in the fraction of variance explained in Set1 and Set2 is attributed to the artificial trend in F13 and F15 and the EIA drift effect.

Examination of the trends of the zonal means show that the latitude of maximum increase, situated in the subtropics, is found poleward of the LHF maximum in the tropic. This pattern is consistent with the expansion of the Hadley Circulation associated with global warming as predicted in climate models (Lu et al., 2007).

The EOF2 patterns of Set1 and Set2 are almost identical, both contributed to 4.3% of the variance of the dataset. The association with the El Nino/Southern Oscillation phenomena is corroborated by a high correlation between their time series and an index of the Southern Oscillation (SOI). The patterns for EOF3 and their associated time series are also similar, indicating that both GSSTF2b Set1 and Set2 are useful for examining interannual variability.

5. Acknowledgment

This study is supported by the MEaSUREs Program of NASA Science Mission Directorate-Earth Science Division. The authors are especially grateful to their program manager M. Maiden and program scientist J. Entin for their valuable supports of this research.

6. References

Andersson, A.; Fennig, K.; Klepp, C.; Bakan, S.; Graßl, H. & Schulz, J. (2010). The Hamburg Ocean Atmosphere Parameters and Fluxes from Satellite Data—HOAPS-3. *Earth System Science Data*, Vol. 2, No. 1, pp. 215-234, ISSN 1866-3508

Angell, J. K. (1981). Comparison of Variations in Atmospheric Quantities with Sea Surface Temperature Variations in the Equatorial Eastern Pacific. *Monthly Weather Review*, Vol. 109, No. 4 , pp. 230-243, ISSN 0027-0644

Aubaum, M. H. P.; Hoskins, B. J. & Stephenson, D. B. (2001). Arctic Oscillation or North Atlantic Oscillation. *Journal of Climate*, Vol. 14, No. 16, pp. 3495-3507, ISSN 0894-8755

Atlas, R.; Hoffman, R. N.; Bloom, S. C.; Jusem, J. C. & Ardizzone, J. (1996). A multiyear global surface wind velocity dataset using SSM/I wind observations. *Bulletin of the American Meteorological Society*, Vol. 77, No. 5, pp. 869-882, ISSN 0003-0007

Bentamy, A.; Katsaros, K. B.; Mestas-Nuñez, A. M; Drennan, W. M.; Forder, E. B. & Roquet, H. (2003). Satellite estimates of wind speed and latent heat flux over the global oceans. *Journal of Climate*, Vol. 16, No. 4, pp. 637-656, ISSN 0894-8755

Bunker, A. F. (1976). Computations of surface energy flux and annual air-sea interaction cycle of the north Atlantic Ocean, *Monthly Weather Review*, Vol. 104, No. 9, pp. 1122-1140, ISSN 0027-0644

Cayan, D. R. (1992). Latent and sensible heat flux anomalies over the Northern Oceans: The connection to monthly atmospheric circulation. *Journal of Climate*, Vol. 5, No. 4, pp. 354-369, ISSN 0894-8755

Cess, R. D. & Udelhofen, P. M. (2003). Climate change during 1985–1999: Cloud interactions determined from satellite measurements. *Geophysical Research Letters*, Vol. 30, No. 1, 1019, ISSN 0094-8276

Chen, J., Carlson B. E., & Del Genio A. D. (2002). Evidence for strengthening of the tropical general circulation in the 1990s. *Science*, Vol. 295, No. 5556, pp. 838-841, ISSN 0036-8075

Chiu, L. S. & Xing, Y. (2004). Modes of interannual variability of oceanic evaporation observed from GSSTF2. *Gayana: International Journal of Biodiversity, Oceanology and Conservation*, Vol. 68, No. 2, pp. 115-120. ISSN 0717-652X

Chiu, L. S. & Newell, R. E. (1983). Variations of zonal mean sea surface temperature and large-scale air-sea interaction. *Quarterly Journal of the Royal Meteorological Society*, Vol. 109, No. 459, pp. 153-168, ISSN 0035-9009

Chiu, L. S.; Chokngamwong, R.; Xing, Y.; Yang, R. & Shie, C.-L. (2008). Trends and Variations of Global Oceanic Evaporation Datasets from Remote Sensing. *Acta Oceanologica Sinica*, Vol. 27, No. 3, pp. 1-12, ISSN 0253-505X

Chou, S.-H. (1993). A comparison of airborne eddy correlation and bulk aerodynamic methods for ocean-air turbulent fluxes during cold-air outbreaks. *Boundary-Layer Meteorology*, Vol. 64, No. 1-2, pp. 75-100, ISSN 0006-8314

Chou, S.-H.; Shie, C.-L.; Atlas R. M. & Ardizzone, J. (1997). Air-sea fluxes retrieved from special sensor microwave imager data. *Journal of Geophysical Research*, Vol. 102, No. C6, pp. 12706-12726, ISSN 0148-0227

Chou, S.-H., Atlas R. M., Shie C.-L. & Ardizzone J. (1995). Estimates of surface humidity and latent heat fluxes over oceans from SSM/I data. *Monthly Weather Review*, Vol. 123, No. 8, pp. 2405-2425, ISSN 0027-0644

Chou, S.-H.; Nelkin, E.; Ardizzone, J.; Atlas, R. & Shie, C.-L. (2001). The Goddard Satellite-Based Surface Turbulent Fluxes Dataset Version 2 (GSSTF2.0) [global (grid of 1° x 1°) daily air-sea surface fluxes from July 1987 to December 2000]. Available from <http://disc.gsfc.nasa.gov/precipitation/gsstf2.0.shtml>

Chou, S.-H.; Nelkin, E.; Ardizzone, J.; Atlas, R. M. & Shie, C.-L. (2003). Surface turbulent heat and momentum fluxes over global oceans based on the Goddard satellite retrieval, version 2 (GSSTF2). *Journal of Climate*, Vol. 16, No. 20, pp. 3256-3273, ISSN 0894-8755

da Silva, A. M.; Young, C. C. & Levitus, S.(1994). *Atlas of Surface Marine Data. Vol. 3: Anomalies of Heat and Momentum Fluxes*. NOAA/NESDIS, Washington, D.C., USA

Deser, C. (2000). On the teleconnectivity of the "Arctic oscillation". *Geophysical Research Letters*, Vol. 27, No. 6, pp. 779-782, ISSN 0094-8276

Esbensen, S. K. & Kushnir,V. (1981). *The heat budget of the global oceans: An atlas based on estimates from marine surface observations*. Climatic Research Institute, Report No. 29, Oregon State University, 27 pp

Fairall, C. W.; Bradley, E. F.; Rogers, D. P.; Edson, J. B. & Young, G. S. (1996). Bulk parameterization of air-sea fluxes for Tropical Ocean Global Atmosphere Coupled Ocean-Atmosphere Response Experiment. *Journal of Geophysical Research*, Vol. 101, No. C2, pp. 3747-3764, ISSN 0148-0227

Fairall, C. W.; Bradley, E. F.; Hare, J. E.; Grachev, A. A. & Edson, J. B. (2003). Bulk parameterization of air-sea fluxes: Updates and verification for the COARE algorithm. *Journal of Climate*, Vol. 16, No. 4, pp. 571-591 , ISSN 0894-8755

Grassl, H.; Jost, V.; Kumar, R.; Schulz, J.; Bauer P. & Schluessel, P. (2000). *The Hamburg Ocean-Atmosphere Parameters and Fluxes from Satellite Data (HOAPS): A climatological atlas of satellite-derived air-sea interaction parameters over oceans.* Max Planck Institute for Meteorology, Report No. 312, ISSN 0937-1060, Hamburg, Germany

Hastenrath, S. (1980). Heat budget of tropical ocean and atmosphere. *Journal of Physical Oceanography*, Vol. 10, No. 2, pp. 159-170, ISSN 0022-3670

Hilburn, K. A. & Shie, C.-L. (2011). Decadal trends and variability in Special Sensor Microwave Imager (SSM/I) brightness temperatures and Earth incidence angle. Report No. 092811, Remote Sensing Systems, 53 pp

Huang, N. E.; Shen, Z.; Long, S. R.; Wu, M. C.; Shih, H. H.; Zheng, Q.; Yen, N.-C.; Tung, C. C. & Liu, H. H. (1998). The empirical mode decomposition and the Hilbert spectrum for nonlinear and non-stationary time series analysis. *Proceedings of the Royal Society of London. Series A*, Vol. 454, No. 1971, pp. 903-995, ISSN 1364-5021

Hsiung, J. (1985). Estimates of global oceanic meridional heat transport. *Journal of Physical Oceanography*, Vol. 15, No. 11, pp. 1405-1413, ISSN 0022-3670

Hurrell, J. W.; Kushnir, Y.; Ottersen, G. & Visbeck, M. (Eds.). (2003). *The North Atlantic Oscillation-Climatic Significance and Environmental Impact*, Geophysical Monograph Vol. 134, American Geophysical Union, ISBN 0-875-90994-9, Washington D.C., USA

Isemer, H.-J. & Hasse, L. (1985). *The Bunker Climate Atlas of the North Atlantic Ocean: 1. Observations*. Springer-Verlag, ISBN 0-387-15568-6, New York, USA

Isemer, H.-J. & Hasse, L. (1987). *The Bunker climate atlas of the North Atlantic Ocean: 2. Air-sea interactions*. Springer-Verlag, ISBN 0-387-17594-6, New York, USA

Josey, S. A.; Kent,E. C. & Taylor,P. K. (1998). *The Southampton Oceanography Centre (SOC) Ocean-Atmosphere Heat, Momentum and Freshwater Flux Atlas*. Southampton Oceanography Centre, Report No.6, Southampton, United Kingdom

Kubota, M.; Ichikawa, K.; Iwasaka, N.; Kizu, S.; Konda, M. & Kutsuwada, K. (2002). Japanese Ocean Flux Data Sets with Use of Remote Sensing Observations (J-OFURO). *Journal of Oceanography*, Vol. 58, No. 1, pp. 213-225, ISSN 0916-8370

Liu, W. T.; Katsaros, K. B. & Businger,J. A. (1979). Bulk Parameterizations of Air-Sea Exchanges of Heat and Water Vapor Including Molecular Constraints at the Interface. *Journal of Atmospheric Science*, Vol. 36, No. 9, pp. 1722-1735, ISSN 1520-0469

Lu, J.; Vecchi, G. & Reichler, T. (2007). The expansion of the Hadley Cell under global warming. *Geophysical Research Letters*, Vol. 34, L06805, ISSN 0094-8276

Murray, F. W. (1967). On the computation of saturation vapor pressure. *Journal of Applied Meteorology*, Vol. 6, No. 1, pp. 203-204, ISSN 0021-8952

Mitas, C. M. & Clement, A. (2005). Has the Hadley cell been strengthening in recent decades?. *Geophysical Research Letters*, Vol. 32, L03809, ISSN 0094-8276

North, G. R.; Bell, T. L.; Cahalan, R. F. & Moeng, F. J. (1982). Sampling Errors in the Estimation of Empirical Orthogonal Functions. *Monthly Weather Review*, Vol. 110, No. 7, pp. 699-706, ISSN 0027-0644

Oberhuber, J. M. (1988). *An Atlas Based on the 'COADS' Data Set: The Budgets of Heat, Buoyancy and Turbulent Kinetic Energy at the Surface of the Global Ocean*. Max-Planck-Institut für Meteorologie, Report No. 15, Hamburg, Germany

Renfrew, I. A.; Moore, G. W. K.; Guest, P. S. & Bumke, K. (2002). A comparison of surface layer and surface turbulent flux observations over the Labrador Sea with ECMWF analyses and NCEP reanalyses. *Journal of Physical Oceanography*, Vol. 32, No. 2, pp. 383-400, ISSN 0022-3670

Reynolds, R. W. & Smith, T. S. (1994). Improved global sea surface temperature analyses using optimum interpolation. *Journal of Climate*, Vol. 7, No. 6, pp. 929-948, ISSN 0894-8755

Reynolds, W. R.; Rayner, N. A.; Smoth, T. M.; Stokes, D. C. & Wang, W. (2002). An improved in situ and satellite SST analysis for climate. *Journal of Climate*, Vol. 15, No. 13, pp. 1609-1625, ISSN 0894-8755

Sakurai, T.; Kurihara, Y. & Kuragano, T. (2005). Merged satellite and in-situ data global daily SST. *Procceeding of International Geoscience and Remote Sensing Symposium*, pp. 2606-2608, ISBN 0-7803-9050-4, Seoul, South Korea, November 14, 2005

Schlussel, P.; Schanz, L. & Englisch, G. (1995). Retrieval of latent-heat flux and longwave irradiance at the sea-surface from SSM/I and AVHRR measurements. *Advances in Space Research*, Vol. 16, No. 10, pp. 107-116, ISSN 0273-1177

Shie, C.-L.; Chiu, L. S.; Adler, R.; Nelkin, E.; Lin, I-I; Xie, P., Wang, F-C; Chokngamwong, R.; Olson, W. & Chu, A. D. (2009). A note on reviving the Goddard Satellite-based Surface Turbulent Fluxes (GSSTF) dataset. *Advances in Atmospheric Sciences*, Vol. 26, No. 6, pp. 1071-1080, ISSN 0256-1530

Shie, C.-L.; Chiu, L. S.; Adler, R.; Lin, I-I; Nelkin, E. & Ardizzone, J. (2010). The Goddard Satellite-Based Surface Turbulent Fluxes Dataset --- Version 2b (GSSTF2b), In: *NASA Goddard Earth Sciences (GES) Data and Information Services Center (DISC)*, October 2010, Available from
<ftp://aurapar1u.ecs.nasa.gov/data/s4pa/GSSTF/> or
<http://disc.sci.gsfc.nasa.gov/daac-bin/DataHoldingsMEASURES.pl?PROGRAM_List=ChungLinShie>

Shie, C.-L. (2010). Science background for the reprocessing and Goddard Satellite-based Surface Turbulent Fluxes (GSSTF2b) Data Set for Global Water and Energy Cycle Research, In: *NASA GES DISC*, 18 pp, October 12, 2010, Available from < http://disc.sci.gsfc.nasa.gov/measures/documentation/Science-of-the-data.pdf>

Shie, C.-L. & Hilburn, K. (2011). A satellite-based global ocean surface turbulent fluxes dataset and the impact of the associated SSM/I brightness temperature, *Proceedings of The 2011 EUMETSAT Meteorological Satellite Conference*, Oslo, Norway, September 5-9, 2011

Shie, C.-L.; Hilburn, K. A.; Chiu, L. S.; Adler, R.; Lin, I-I; Nelkin, E. & Ardizzone, J. (2011). The Goddard Satellite-Based Surface Turbulent Fluxes Dataset --- Version 2c (GSSTF2c). In: *NASA GES DISC*, by the end of October 2011.

Tomita, H.; Kubota, M.; Cronin, M. F.; Iwasaki, S.; Konda, M. & Ichikawa, H. (2010). An assessment of surface heat fluxes from J-OFURO2 at the KEO and JKEO sites. *Journal of Geophysical Reserach*, Vol. 115, C03018, ISSN 0148-0227

Walker, G. T. & Bliss, E. W. (1932). World weather V. *Memoirs of the Royal Meteorological Society*, Vol. 4, No. 36, pp. 53-84, LCCN 7021-1603

Wallace, J. M. (2000). North Atlantic Oscillation/annular mode: Two paradigms—one phenomenon. *Quarterly Journal of the Royal Meteorological Society*, Vol. 126, No. 564, pp. 791-805, ISSN 0035-9009

Wallace, M. & Gutzler, D. S. (1981). Teleconnections in the geopotential height field during the Northern Hemisphere winter. *Monthly Weather Review*, Vol. 109, No. 4, pp. 784-812, ISSN 0027-0644

Weare, B. C.; Strub, P. T. & Samuel, M. D. (1981). Annual Mean Surface Heat Fluxes in the Tropical Pacific Ocean. *Journal of Physical Oceanography*, Vol. 11, No. 5, pp. 705-717, ISSN 0022-3670

Wentz, F. J. (1997). A well calibrated ocean algorithm for Special Senor Microwave/Imager. *Journal of Geophysical Research*, Vol. 102, No. C4, pp. 8703-8718, ISSN 0148-0227

Wentz, F. J.; Ricciardulli, L.; Hilburn K. A. & Mears C. A. (2007). How Much More Rain Will Global Warming Bring? *Science*, Vol. 317, No. 5835, pp. 233-235, Supporting material, ISSN 0036-8075

Wielicki B.; Wong, T.; Allen, R. P.; Slingo, A.; Kiehl, J. T.; Soden, B. J.; Gordon, C. T.; Miller, A. J.; Yang, S.-K.; Randall, D. A.; Robertson, F.; Susskind, J. & Jacobowitz, H. (2002). Evidence for large decadal variability in the tropical mean radiative energy budget. *Science*, Vol. 295, No. 5556, pp. 841-844, ISSN 0036-8075

Xing, Y. (2006). *Recent changes in oceanic latent heat flux from remote sensing*. Ph.D. dissertation, George Mason University, 119 pp

Zeng, X.; Zhao, M. & Dickinson, R. E., (1998). Intercomparison of bulk aerodynamic algorithms for the computation of sea surface fluxes using TOGA COARE and TAO data. *Journal of Climate*, Vol. 11, No. 10, pp. 2628-2644, ISSN 0894-8755

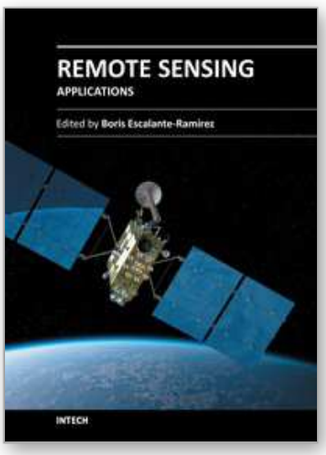

Remote Sensing - Applications
Edited by Dr. Boris Escalante

ISBN 978-953-51-0651-7
Hard cover, 516 pages
Publisher InTech
Published online 13, June, 2012
Published in print edition June, 2012

Nowadays it is hard to find areas of human activity and development that have not profited from or contributed to remote sensing. Natural, physical and social activities find in remote sensing a common ground for interaction and development. This book intends to show the reader how remote sensing impacts other areas of science, technology, and human activity, by displaying a selected number of high quality contributions dealing with different remote sensing applications.

How to reference
In order to correctly reference this scholarly work, feel free to copy and paste the following:

Long S. Chiu, Si Gao and Chung-Lin Shie (2012). Oceanic Evaporation: Trends and Variability, Remote Sensing - Applications, Dr. Boris Escalante (Ed.), ISBN: 978-953-51-0651-7, InTech, Available from: http://www.intechopen.com/books/remote-sensing-applications/oceanic-evaporation-trend-and-variability

INTECH
open science | open minds

InTech Europe
University Campus STeP Ri
Slavka Krautzeka 83/A
51000 Rijeka, Croatia
Phone: +385 (51) 770 447
Fax: +385 (51) 686 166
www.intechopen.com

InTech China
Unit 405, Office Block, Hotel Equatorial Shanghai
No.65, Yan An Road (West), Shanghai, 200040, China
中国上海市延安西路65号上海国际贵都大饭店办公楼405单元
Phone: +86-21-62489820
Fax: +86-21-62489821

IntechOpen